

Article

Generalized Circuit Model of Shielded Capacitive Power Transfer

Suziana Ahmad^{1,2}, Reiji Hattori^{1,*} and Aam Muharam³ 

¹ Interdisciplinary Graduate School of Engineering Sciences, Kyushu University, Fukuoka 816-8580, Japan; binti.ahmad.suziana.749@s.kyushu-u.ac.jp

² Faculty of Electrical and Electronic Engineering Technology, Universiti Teknikal Malaysia Melaka, Melaka 76100, Malaysia

³ Research Centre for Electrical Power and Mechatronics, Indonesian Institute of Sciences, Bandung 40135, Indonesia; aam.muhamaram@lipi.go.id

* Correspondence: hattori@gic.kyushu-u.ac.jp; Tel.: +81-92-583-7887

Abstract: A capacitive power transfer (CPT) system wirelessly transfers energy between coupling plates and performance issues related to CPT systems are resonance conditions, matching impedance, voltage stress, and power loss. A generalized circuit model is proposed for shielded capacitive power transfer (S-CPT) using an algebraic method. The proposed generalized S-CPT model is analyzed based on the symmetric and asymmetric configurations, and the relationship between the parameters of S-CPT is obtained with respect to the resonance condition, matching impedance, voltage stress, and efficiency. The best configuration of a symmetric S-CPT is recommended, and an asymmetric S-CPT is proposed based on the analysis results. Asymmetric-S-CPT hardware was constructed and demonstrated an operating frequency of 13.56 MHz. The hardware experimental result shows the validity and effectiveness of the proposed generalized model for designing S-CPT.

Keywords: capacitive power transfer; modelling; shielded capacitive power transfer



Citation: Ahmad, S.; Hattori, R.; Muharam, A. Generalized Circuit Model of Shielded Capacitive Power Transfer. *Energies* **2021**, *14*, 2826. <https://doi.org/10.3390/en14102826>

Academic Editor: Mauro Mongiardo

Received: 14 April 2021

Accepted: 11 May 2021

Published: 14 May 2021

Publisher's Note: MDPI stays neutral with regard to jurisdictional claims in published maps and institutional affiliations.



Copyright: © 2021 by the authors. Licensee MDPI, Basel, Switzerland. This article is an open access article distributed under the terms and conditions of the Creative Commons Attribution (CC BY) license (<https://creativecommons.org/licenses/by/4.0/>).

1. Introduction

Capacitive power transfer (CPT) is a wireless power transfer technology that has attracted attention among researchers. A CPT system uses coupling plates that act as a capacitor to transfer the AC voltage wirelessly from the transmitter side to the load. Recently, CPT systems have been developed by many researchers in many applications, such as electric vehicle charging [1–4], medical devices [5], unmanned aerial vehicles [6,7], and rotary applications [8–11]. Recently, a variety of CPT systems have been introduced with different capacitive plate, compensation circuit, and inverter designs to achieve the best performance and efficiency of the power delivery. CPT systems feature cost effectiveness, light weight, and good tolerance to misalignment [12].

In CPT technology, modeling of the CPT system has been performed to study the behavior of the circuit covers to find the best solution for the efficiency, resonance condition, mismatch of the coupler, and other problems. Different types of analysis and modeling of CPT systems have been introduced in previous studies, including finite element modeling of the capacitive coupler [5], the duality principle of the primary and secondary side [13], multiple input with single output [14], and an induced voltage source model by using six coupling-dependent capacitors between each pair of plates [15].

The structure of the capacitive coupler has been fabricated in various designs such as a two-plate structure, four-plate parallel structure, four-plate stacked structure, and six plate structure [12]. Thus, the capacitance between the plates is different and needs to be simplified in an equivalent circuit. In a CPT system with four plates [16], the plates are arranged in parallel to form the coupling capacitance, as illustrated in Figure 1a, and the plates can be arranged in a horizontal plane in regard to the application [17,18]. Figure 1a

shows the four-plate structure in which two plates are on the primary and secondary side. Typical coupling capacitance in the CPT system with four plates can be modeled as two coupling capacitors with input and output voltage, as shown in Figure 1b. In a previous study, a generalized coupling model using the duality principle was proposed [13] to overcome the drawback of the two-capacitor coupling model, as shown in Figure 1b, in which the primary and secondary side of the coupling plate cannot be analyzed separately and there is complexity in the analysis when coupling plates are not exactly in parallel.

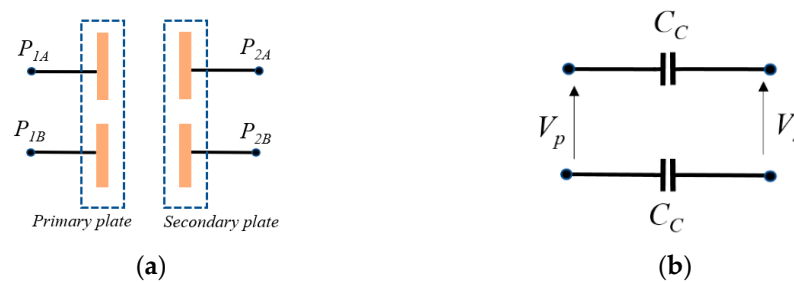


Figure 1. Plate structure. (a) Four-plate structure, (b) normal capacitive coupling model.

The four-plate structure has been analyzed in various capacitive coupling models. Six coupling capacitors can be formed in the four-plate structure and can be simplified into an equivalent two-port model [17] and π -topology circuit [16,19]. The six-capacitor model can be divided into mutual capacitance, primary capacitance, and secondary capacitance in which the capacitive coupling factor has been introduced into the model [13]. The mutual coupling model used without the grounding effect to describe the four-plate parallel structure of the CPT system is inaccurate and it has been found that the CPT system performance is effected by grounding [20].

In the CPT system, there is a need for a compensation resonant topology in which it is used to establish resonances in the circuit and to transfer a high level of power [19]. Many resonant compensation topologies have been introduced in the CPT system, such as LC [17,21], LCL [19], and LCLC [18] topology. Thus, both the compensation circuit and the capacitance coupler can be formed into an equivalent CPT model for analysis purposes. The fundamental harmonic approximation (FHA) method has been proposed to analyze the CPT circuit with an LC compensation circuit in which voltage-dependent current sources represent the capacitive coupling between the primary and secondary sides for a four-plate horizontal structure of the CPT system.

The six-plate structure has been introduced in the CPT system [22] in which two plates and four plates act as shielding plates and coupler plates, respectively. In comparison to the four-plate structure, a six-plate coupler has the advantages of safety and electric field emission reduction [2,23]. The six-plate structure can be formed into a 15-coupling capacitor model with self and mutual capacitance [23].

This work is focuses on the behavior of the circuit with four coupler plates and two shielding plates in which the couplers build the six-plate structure. Modeling and designing the CPT system can become complex based on the coupler structure. Moreover, the included compensation circuit in the CPT system makes the analysis more difficult. In this report, a generalized model is proposed with deep analysis of the parameter variation. Therefore, the parameters of S-CPT can be determined regarding the design specification such as high- and low-power applications, safety regulations, and different load outputs. Moreover, the effect on the S-CPT system can be predicted when the slightest change in parameters occurs. The new findings are presented to address the best solution for the resonance conditions, impedance matching conditions, and efficiencies in shielded capacitive power transfer (S-CPT). The findings are as follows.

- An analysis method was developed to design a generalized model of an S-CPT system using an algebraic method in a linear system in symmetric and asymmetric configurations.
- A configuration of the symmetric S-CPT based on the analysis method is recommended based on the resonance condition, matching impedance, voltage stress, and efficiency.
- A configuration of an asymmetrical S-CPT system with hardware validity is proposed.

2. Modeling of an S-CPT System

S-CPT with a symmetrical configuration was introduced in previous research [24,25]. However, a full analysis of the S-CPT system based on the electrical behavior of the circuit has not yet been performed. Thus, in this section, a full analysis is presented in which the best S-CPT design is obtained in terms of the resonance conditions and impedance matching conditions by using an algebraic method for a linear system. The detailed analysis is explained based on the S-CPT model shown in Figure 2.

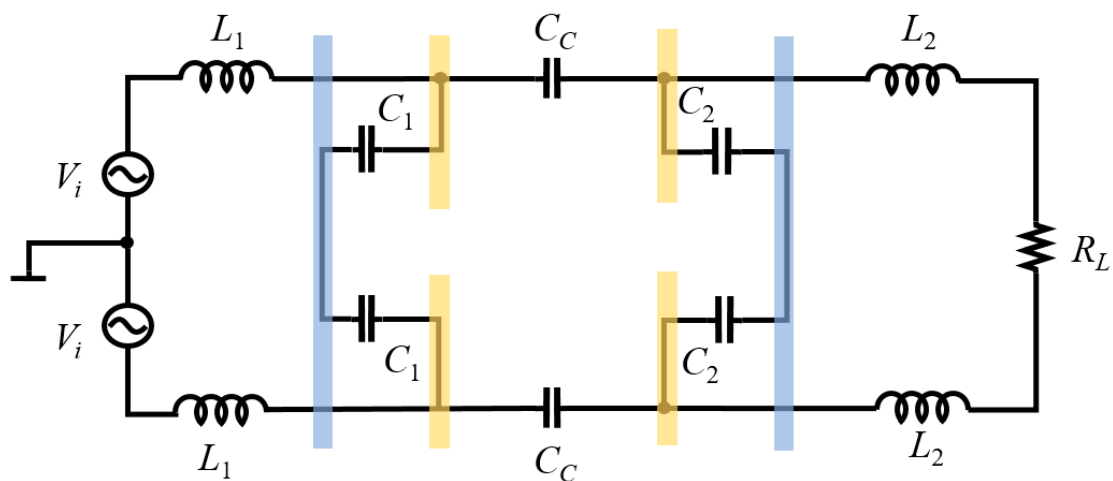


Figure 2. Equivalent circuit schematic for S-CPT.

Figure 2 shows the S-CPT system model, which consists of a coupling capacitor C_C between the transmitter and receiver. The S-CPT system is constructed as a four-plate structure with two shielding plates. L_1 and C_1 are the series resonance inductor and shield coupler capacitance on the transmitter side, respectively. On the receiver side, the series resonance inductor L_2 and shield coupler C_2 are connected to the load R_L . In addition, the AC supply V_i is used in the circuit as the input. Analysis of the circuit is based on the ideal S-CPT system in which the internal resistances of the inductor, capacitance, voltage supply, and others are assumed to be zero.

2.1. Equivalent Model of Generalized S-CPT

The S-CPT shown in Figure 2 can be simplified into Figure 3 for analysis purposes. The analysis uses the algebraic method and S-CPT system as a linear system.

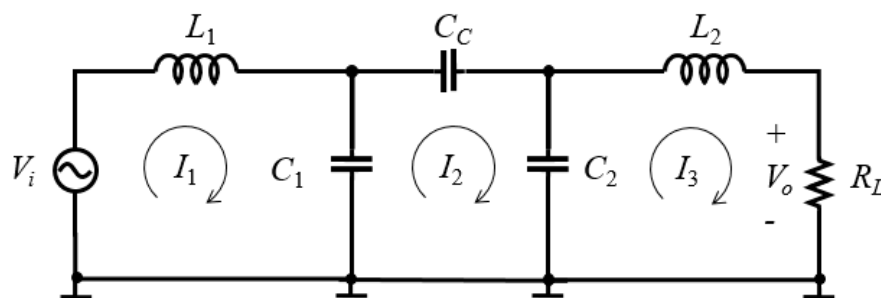


Figure 3. Simplified equivalent circuit for S-CPT.

Figure 3 shows the circuit of the S-CPT system, and Kirchoff’s current law is used for each loop for analysis purposes, with values of reactance parameters represented by $j\omega$, where ω is the angular frequency. The equations for each loop are obtained as follows:

$$\begin{bmatrix} (j\omega L_1 + \frac{1}{j\omega C_1}) & -\frac{1}{j\omega C_1} & 0 \\ -\frac{1}{j\omega C_1} & (\frac{1}{j\omega C_1} + \frac{1}{j\omega C_C} + \frac{1}{j\omega C_2}) & -\frac{1}{j\omega C_2} \\ 0 & -\frac{1}{j\omega C_2} & (j\omega L_2 + \frac{1}{j\omega C_2} + R_L) \end{bmatrix} \begin{bmatrix} I_1 \\ I_2 \\ I_3 \end{bmatrix} = \begin{bmatrix} V_i \\ 0 \\ 0 \end{bmatrix} \quad (1)$$

Equation (1) is solved by substituting I_2 and I_3 into I_1 ; then, the current I_1 can be obtained as Equation (2). The angular frequency $\omega = 2\pi f$, where f represents the value of the operating frequency in the S-CPT system and r is the ratio of the secondary inductor C_2 to C_1 .

$$I_1 = \frac{j\omega C \{ -\omega^2 M C L_2 + N + j\omega M C R_L \}}{[\omega^4 M C^2 L_1 L_2 + \omega^2 C \{ M C R_0 R_L + N L_1 + Q L_2 \} + T] - j[\omega^3 M C^2 \{ L_1 R_L + L_2 R_0 \} - \omega C \{ Q R_L + N R_0 \}]} V_i, \quad (2)$$

where

$$\begin{bmatrix} M \\ N \\ Q \\ T \end{bmatrix} \equiv \begin{bmatrix} ar^2 \\ (ar - 1) \\ (a - 1)r^2 \\ (ar - r - 1) \end{bmatrix}, \quad (3)$$

and the capacitance C is equal to the primary capacitance, $C = C_1$, the ratio of the primary capacitance to the secondary capacitance $r = C_2/C_1$, and the relationship between the coupling capacitance and the shield coupler $a = 1 + C/C_C + 1/r$.

First, in an S-CPT system with a resonance condition, the total impedance is purely resistive, in which the imaginary part is zero. In a CPT circuit, resonance occurs when the total impedance of inductance is equal to the total impedance of capacitance and, as a result, the total impedance of the circuit is equal to the resistive value only. Thus, using $|I_1/V_i|$ in Equation (2), the correlation between the primary inductor L_1 and other components under the resonance condition is obtained by Equation (4).

$$L_1 = \frac{b C r^2 R_L^2 (a - 1) + \{ b L_2 - (ar - 1) \} \{ (1 - \frac{1}{a}) b L_2 - (ar - 1) + r \}}{b^2 C R_L^2 + \omega^2 C \{ b L_2 - (ar - 1) \}^2}, \quad (4)$$

where

$$b \equiv \omega^2 a r^2 C. \quad (5)$$

Second, in an S-CPT system with a matching condition, the internal resistance of the source load, 50Ω , is equal to the load [24]. As a result, the current magnitude $|I_1/V_i|$ in the matching condition of the S-CPT system gives a magnitude value of 0.01 or 1/100 with an effective load R_L' of 100Ω . In the next section, the analysis findings for the S-CPT system are discussed in detail.

2.2. Ratio Analysis Model

In resonance conditions, the correlation between the primary inductor L_1 and other parameters was obtained, and further analysis was conducted. The analysis was performed to study the effect on the L_1 value when the load changes based on the ratio between the coupling capacitance and when both the primary and the secondary shield coupler capacitance is 1. Thus, the parameters used for the ratio analysis are listed in Table 1 with an operating frequency of 13.56 MHz. One of the specific industry, scientific, and medical (ISM) band frequencies for consumer devices determined by ITU-K is 13.56 MHz and it has no negative impact on other licensed bands [24]. Furthermore, the size and value of inductance in the CPT system can be decreased when the frequency is increased [26]. Therefore, 13.56 MHz is selected as the operating frequency in this work.

Table 1. Circuit parameters for ratio analysis.

| Parameter | Symbol | Value | Unit |
|--------------------------------------|--------|---------------------|------|
| Primary shield coupler capacitance | C_1 | 10^{-12} | F |
| Secondary shield coupler capacitance | C_2 | 10^{-12} | F |
| Coupling capacitance | C_C | 10^{-12} | F |
| Operating frequency | f | 13.56×10^6 | Hz |

The relationship of the primary inductor L_1 to the secondary inductor L_2 with the same value of coupling capacitance C_C and shield coupler capacitance in the primary, C_1 , and secondary, C_2 , sides are formalized by graph transformation, as shown in Figure 4, which illustrates L_1 and L_2 in the resonance condition with the variation of the load R_L . This graph can be used to estimate the value of the S-CPT parameter during the design process.

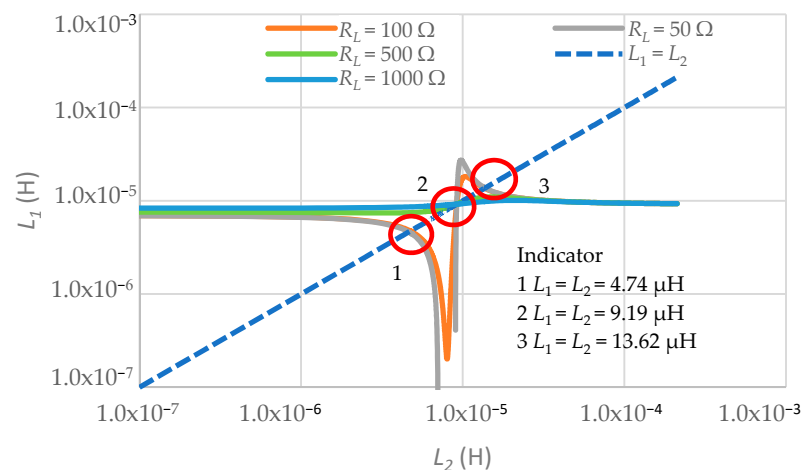


Figure 4. Relationships between L_1 and L_2 as a parameter of R_L .

3. Designing a Symmetric S-CPT

Based on Equations (1), (2) and (4), a symmetric S-CPT can be designed to meet the requirements of the resonance conditions and matching impedance conditions. Thus, based on Figure 4, a symmetric S-CPT system is the configuration in which the value of the primary inductor is equal to that of the secondary inductor; mathematically, it can be written as $L_1 = L_2$. Moreover, the values of the primary and secondary capacitances are the same ($C_1 = C_2$) to form a symmetric configuration of the S-CPT system. In this section, the design of the symmetric S-CPT system is analyzed by using a ratio analysis method, as in the previous section.

3.1. Resonance Conditions of the Symmetric S-CPT

Resonance in the CPT system can be created using an inductor in which it is connected to capacitive coupler [17,27]. Based on the finding of the correlation of L_1 , the symmetric S-CPT can be designed with the value of the inductor, $L_1 = L_2$, and capacitance, $C_1 = C_2$. The graph in Figure 4 is therefore made up of a straight line to represent the symmetric S-CPT case. Thus, as the straight line for the symmetric S-CPT intersects with other plotted lines, three numerical values are shown on the graph. Therefore, there are three values of L_1 and L_2 of the symmetric S-CPT system that can be used in the design for the same load R_L . These three values are represented by points 1, 2, and 3 in Figure 4.

At points 1 and 3, L_1 and L_2 change with the value of R_L . However, there is no intersection at points 1 and 3 for the higher R_L at 500 and 1000 Ω . At point 2, both L_1 and L_2 remain the same, even though R_L changes. Therefore, the value of L_1 is not affected by R_L . In designing the symmetric S-CPT system for a load of 100 Ω , three points of intersections, as shown in Figure 4, indicate that the values of L_1 and L_2 occurred at 4.74, 9.19, and 13.62 μH . Therefore, these inductor values can be used in the S-CPT system. However, for a better analysis, the impedance matching conditions must be considered for these values.

3.2. Matching Condition of the Symmetric S-CPT

Based on previous work [24], the optimal impedance matching occurs when the effective load R_L' is twice the value of the internal resistance R_o or can be written as $R_L' = 2R_o$. The impedance matching will take place between the specific load resistance and internal resistance R_o in which maximum power transfer can be achieved in the CPT system [28]. Based on the analysis, the current magnitude peak $|I_1/V_i|$ is $1/R_L'$ or 0.01. In this matching condition, there is no reflection of the signal from the load, and the power can be transferred to the maximum value. Thus, for the internal resistance of the power supply $R_o = 50 \Omega$, R_L' must be 100 Ω . By using Equation (2) with the parameters in Table 1, $|I_1/V_i|$ is plotted for $L_1 = L_2$ of 4.74, 9.19, and 13.62 μH for the load, R_L is 100 Ω , and the plotted graph is as shown in Figure 5.

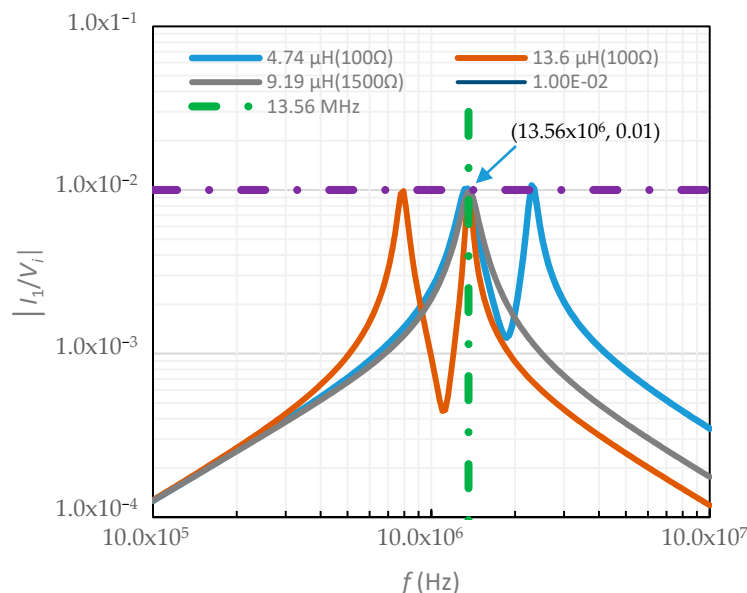


Figure 5. Matching condition of the symmetric CPT with inductance values of 4.74, 9.19, and 13.62 μH .

Figure 5 shows the current magnitude $|I_1/V_i|$ for the inductor values 4.74, 9.19, and 13.62 μH . In addition, the line graphs are drawn with values of 0.01 and 13.56 MHz to indicate the $|I_1/V_i|$ peak value and operating frequency value, respectively. The resulting graph shows that the values of S-CPT with inductances of 4.74 and 13.62 μH reach a peak of 0.01 S at an operating frequency of 13.56 MHz with a load of 100 Ω . However, S-CPT

with an inductance value of 9.19 μH peaks at 0.01 S when the load R_L approximates to 1500 Ω to obtain an effective load R_L' of 100 Ω . In summary, for S-CPT with inductances of 4.74 and 13.62 μH , R_L' is equal to R_L to meet the matching condition requirement. In contrast, the S-CPT with a 9.19 μH inductor reaches the matching impedance condition with an R_L of 1500 Ω .

3.3. Voltage Stress Condition of the Symmetric of S-CPT

The coupler plate and shield coupler can be constructed using a printed circuit board (PCB) with a cuprum surface. The PCB faced a breakdown voltage when the applied electric field strength on the PCB surface exceeded a certain threshold [29] depending on the PCB material. Several factors influence the breakdown voltage, such as atmospheric condition, structure of the air gap, and voltage waveform [30].

Moreover, the air also has a dielectric strength or a maximum electric field of 30 kV/cm, and it has been found that, with a voltage limit of 30 kV/cm, the gap between the shield and coupler must be designed under the limitation value [24]. In the S-CPT system, the shield plate minimizes the electric field emission from the coupler plates to the air [2]. In designing for high-voltage applications of S-CPT, the breakdown voltage must be considered. The maximum breakdown voltage is proportional to the air dielectric strength E_{SC} and the gap between the plates. The maximum breakdown voltage can be written as

$$V_A = E_{SC}d_{sc} \quad (6)$$

and

$$C_1 = \frac{\epsilon_r \epsilon_0 A_{SC}}{d_{SC}}, \quad (7)$$

where V_A and d_{SC} are the voltage stress and gap between the plates, respectively. The capacitance value C_1 is directly proportional to the dielectric constant of the material ϵ_r , the dielectric constant of free space ϵ_0 , the area of the capacitance plate A_{SC} , and gap between the coupling electrodes, d_{SC} . Reducing the gap between the plates decreases the breakdown voltage between the plates. In the design specification for transferring high voltage, the voltage stress between the plates must be considered for safety reasons.

Coupler plates of 10 pF, as shown in Table 1, can be fabricated using (7) with an area of the plate of 60 cm^2 , air as the dielectric material, and a gap between the plates of 0.53 cm. Therefore, the breakdown voltage between the fabricated coupler can be determined using (6) and the calculated breakdown voltage is 15.90 kV for air dielectric strength E_{SC} of 30 kV/cm. Considering 50% safety tolerance of the breakdown voltage, the applied voltage stress between the plates must be under 7.95 kV.

An analysis of an S-CPT symmetric circuit at 4.74, 9.19, and 13.62 μH was done to investigate the voltage stress at the coupling shield plate primary side, coupling shield plate secondary side, and coupling plate. This analysis was intended to address concerns about breakdown voltage.

Figures 6–8 show the voltage changes at the coupling plate in which V_A and V_B are coupling shield voltages by injecting a voltage input of 1 V at the primary and secondary voltages, respectively. The voltage difference between V_B and V_A refers to the coupling voltage.

Figure 6 shows that a higher voltage occurs at coupling voltage $V(V_A, V_B)$ when $L_1 = L_2 = 4.74 \mu\text{H}$ when the maximum amplitude voltage is 7.72 V. In designing S-CPT with safety considerations, voltage input can be increased as long as the coupling voltage $V(V_A, V_B)$ is under the breakdown voltage of 7.95 kV. Figure 7 shows that the highest voltage occurred at the coupling shield in the primary side $V(V_A)$. Considering Figure 7 with the ratio value, when the voltage stress at the coupling shield $V(V_A)$ is approaching the breakdown voltage, voltage stresses at both $V(V_A, V_B)$ and $V(V_B)$ are still in a safe condition. In addition, Figure 8 indicates that the voltage stress of the coupling shield plates at the primary and secondary sides are both high in magnitude. Thus, the voltage stress between coupling plates is low and results in a low current.

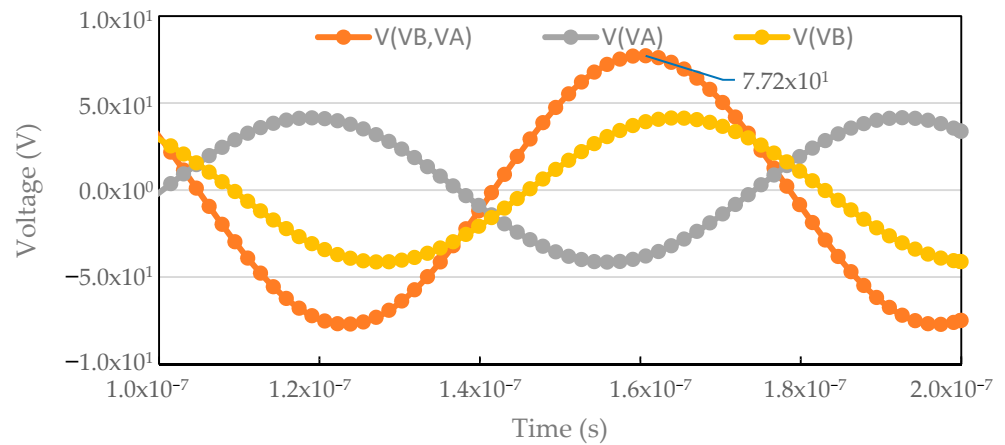


Figure 6. Voltage stress for $L_1 = L_2 = 4.74 \mu\text{H}$.

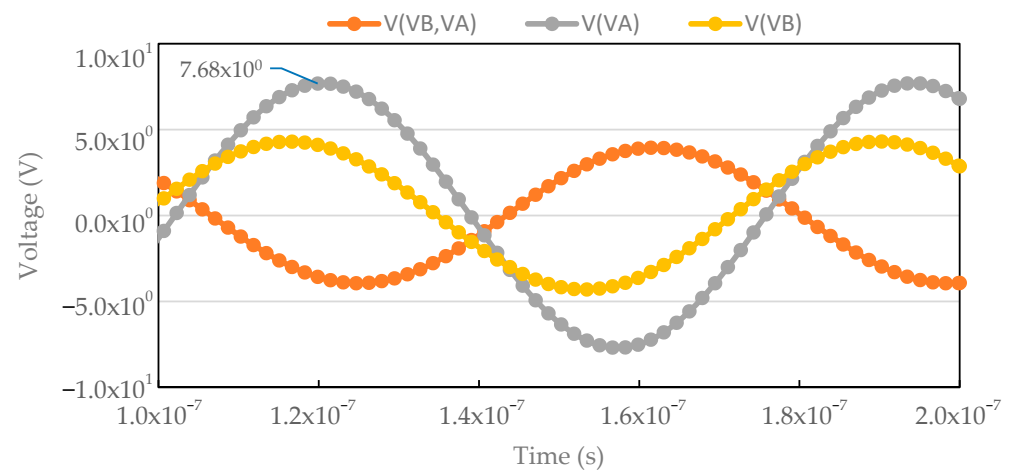


Figure 7. Voltage stress for $L_1 = L_2 = 9.19 \mu\text{H}$.

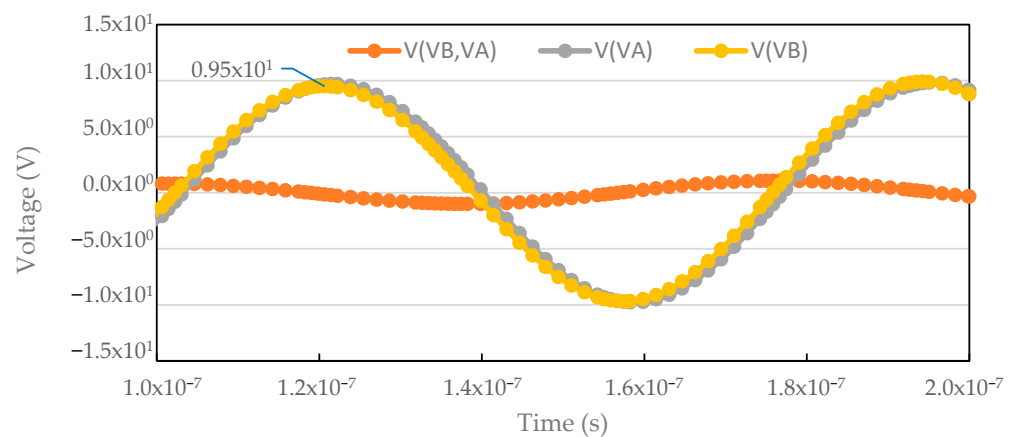


Figure 8. Voltage stress for $L_1 = L_2 = 13.62 \mu\text{H}$.

In summary, $L_1 = L_2 = 4.74 \mu\text{H}$ can be used in designing a symmetric S-CPT system because of the lowest value of inductance. The low value results in a small inductor size as well as a low price. Moreover, the results show that the voltage stress is higher at the coupling plate.

3.4. Efficiency Condition of the Symmetric S-CPT

An inductor has internal resistance, which contributes to the loss. Power loss in inductors reduces the CPT system efficiency [18]. The relationship between the internal resistance of the inductor and R_S [24] can be written as follows.

$$R_S = \frac{8\rho}{\phi^2} \sqrt{\frac{2RL}{\mu}} \quad (8)$$

where ρ , μ , and ϕ are the resistivity, core material permeability, and thickness of the wire, respectively, and R is the radius of the core. Equation (8) shows that R_S is directly proportional to the inductance. The higher the value of the inductor, the higher the value of the internal resistance, because the resultant loss increases in the S-CPT system and reduces the system efficiency. For the same material and radius of the inductance, a higher inductance is a drawback in terms of the power loss. For analysis purposes, the internal resistance R_S is calculated based on the inductor material and diameter being the same with an air-core-type inductor to investigate the effect of the internal series on the S-CPT system efficiency. The approximate efficiency EFF in the S-CPT system is presented in Figure 9.

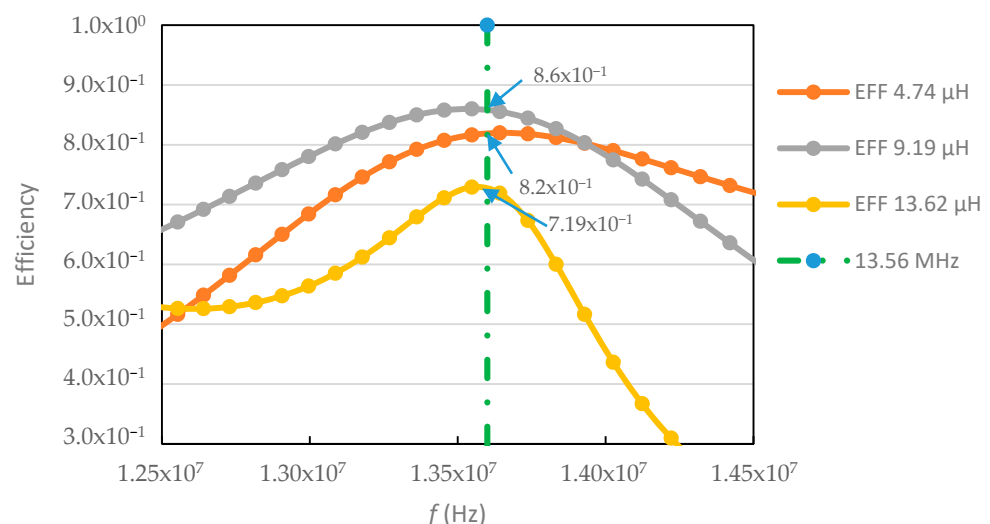


Figure 9. Efficiency in S-CPT with internal resistance of the inductor.

Figure 9 shows the approximate value of efficiency for $L_1 = L_2$ for 4.74, 9.19, and 13.62 μH , and a straight line is drawn for an abscissa of 13.56 MHz. The efficiency of the ideal S-CPT without loss is 1.0, and the graph shows that the power loss drawn by internal series resonance affects the efficiency. Although S-CPT with $L_1 = L_2 = 9.19 \mu\text{H}$ has a higher inductance value than with $L_1 = L_2 = 4.74 \mu\text{H}$, the efficiency of S-CPT with $L_1 = L_2 = 9.19 \mu\text{H}$ is the highest compared with the others, with a value of 0.86. Considering Figure 4, S-CPT with $L_1 = L_2 = 9.19 \mu\text{H}$ has stability and a minimal effect on resistor changes in the system. Thus, an internal series of inductors induces least effect on the efficiency of the S-CPT system with $L_1 = L_2 = 9.19 \mu\text{H}$. In contrast, the highest power loss occurred at $L_1 = L_2 = 13.62 \mu\text{H}$ and affected the efficiency value. The obtained efficiency was 0.72.

3.5. Recommendation for the Symmetric S-CPT Model

The analyses for $L_1 = L_2$ of 4.74, 9.19, and 13.62 μH are presented in terms of the resonance condition, matching condition, electric field limitation, and power loss, as summarized in Table 2.

Table 2. Findings for the symmetric S-CPT based on the analysis method.

| Parameter | Case 1 | Case 2 | Case 3 |
|--------------------------|------------------|---------------|-------------------------|
| $L_1 = L_2$ | 4.74 00B5H | 9.19 μ H | 13.6 μ H |
| Resonance condition | Comply | Comply | Comply |
| Matching condition | Comply | Comply | Comply |
| Load | 50 Ω | 1500 Ω | 50 Ω |
| Electric field radiation | High at V_{CC} | High at V_A | High at V_A and V_B |
| Power loss | 1.8 dB | 1.2 dB | 2.3 dB |

It is recommended that, in designing a symmetric S-CPT system, $L_1 = L_2 = 4.74 \mu\text{H}$ be used for the S-CPT system because of the small inductance value. The small value of inductance makes the system small and light. However, when considering stability in the resonance condition and loss resulting from the internal resistance of the inductance, $L_1 = L_2 = 9.19 \mu\text{H}$ is the most suitable, but the effective load must be obtained. In contrast, $L_1 = L_2 = 13.6 \mu\text{H}$ can be excluded from the design consideration because of the high value of inductance, high loss, and heavy weight.

4. Designing an Asymmetric S-CPT

The behavior of the S-CPT circuit when the secondary inductor L_2 is zero was analyzed, and a new asymmetric S-CPT system was designed. Without the secondary inductor, the S-CPT system can minimize the total S-CPT loss because the total quantity of the inductor in S-CPT is reduced and the efficiency can be increased. By using Equation (1) and the same parameters as in Table 1 with the secondary inductor L_2 equal to zero, the current I_1 and the primary inductor L_1 can be deduced as follows:

$$I_1 = \frac{\omega C \sqrt{N^2 + \omega^2 M C^2 R_L^2}}{\sqrt{[-\omega^2 C \{M C R_0 R_L + N L_1\} + T]^2 + [\omega^3 M C^2 (L_1 R_L) - \omega C \{Q R_L + T R_0\}]^2}} V_i \quad (9)$$

$$L_1 = \frac{b C r^2 R_L^2 (a - 1) + \{-(a r - 1)\} \{-(a r - 1) + r\}}{b^2 C R_L^2 + \omega^2 C \{-(a r - 1)\}^2} \quad (10)$$

Equations (9) and (10) show the relationship between current I_1 and the primary inductor L_1 with other parameters in the asymmetric S-CPT system. Based on this relationship, the performance of the asymmetric S-CPT system was investigated in terms of the resonance condition, matching impedance, electric field limitation, and efficiency.

4.1. In the Resonance Condition of the Asymmetric S-CPT System

In the resonance condition, the relationship between the primary inductor and load, shielded by the coupling plate ratio, and the coupling capacitance based on Equations (9) and (10), are plotted in Figures 10–13.

Figure 10 shows the relationship between L_1 and R_L when the value of $L_2 = 0$. The value of the inductor is stable when the load increases gradually. However, the inductor value drastically increases when the load approaches 100 Ω and becomes stable again when saturated when the frequency increases.

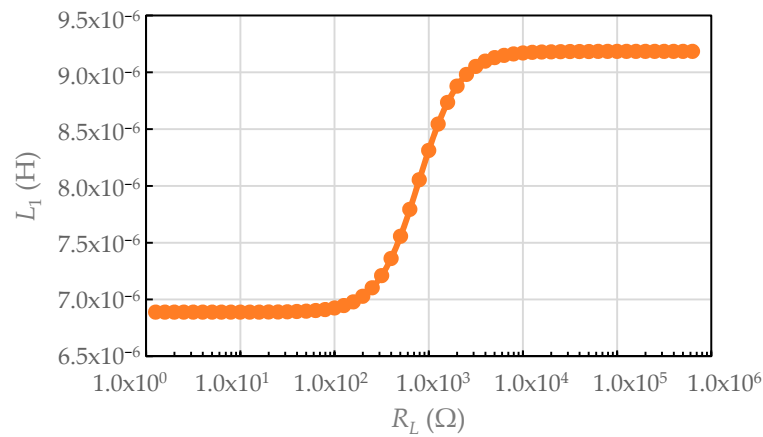


Figure 10. Inductor value L_1 at various load resistances R_L .

Figure 11 shows that the inductor L_1 increases by a small amount when the ratio between the coupling shield plate in the secondary and primary C_2/C_1 increases. Therefore, if misalignment occurs in the coupling shield plate, it does not significantly affect the primary inductor. Thus, the resonance and matching impedance condition change is small.

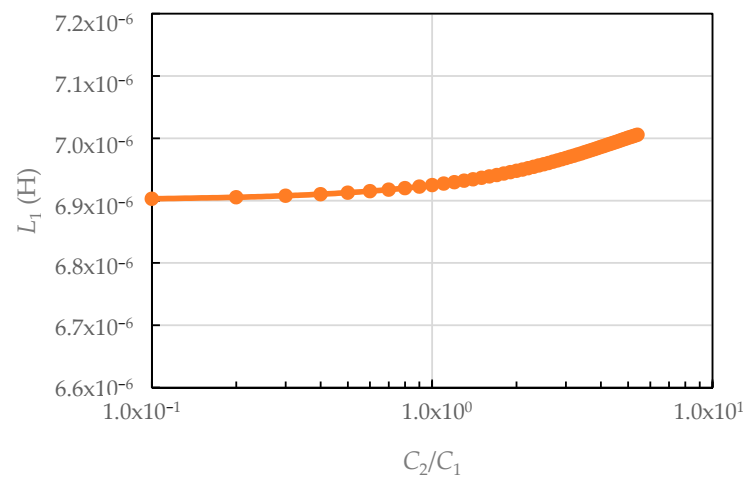


Figure 11. Inductor value L_1 for various ratios of the shielded capacitance C_2/C_1 .

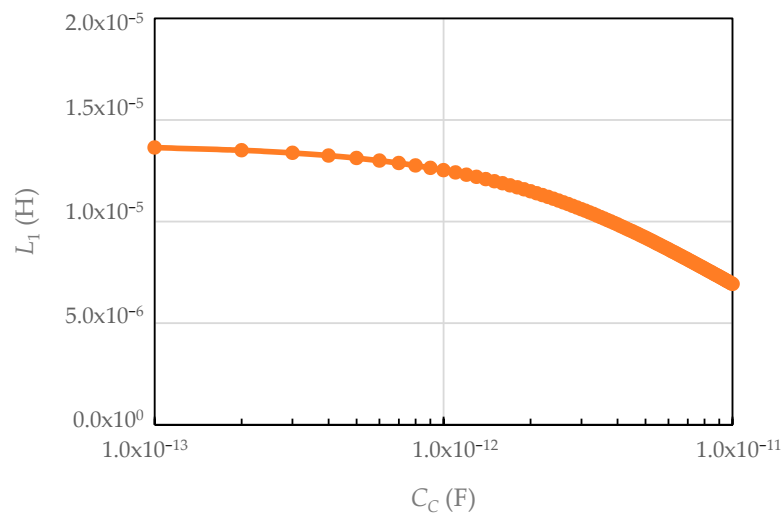


Figure 12. Inductor value L_1 for various ratios of the coupling capacitance C_c .

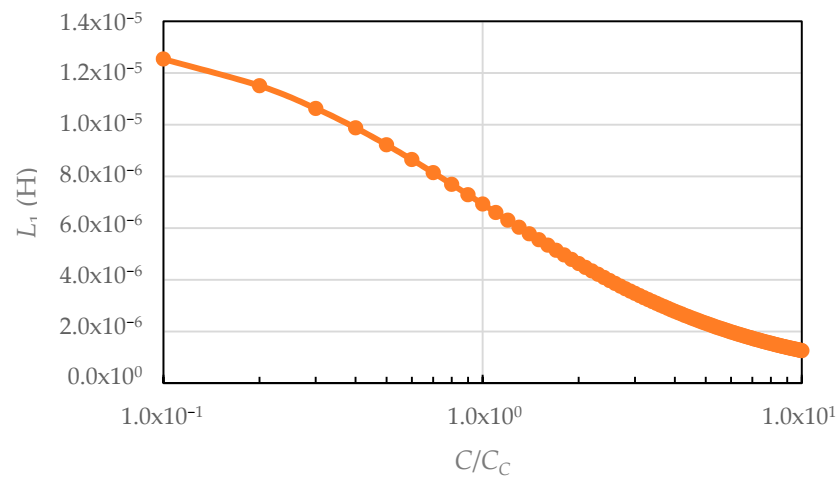


Figure 13. Inductor value L_1 for various ratios of primary capacitance to coupling capacitance.

Figure 12 shows the relationship between the inductor and coupling plate. When the distance of the coupling capacitance plate decreases, the coupling capacitance increases, and the inductor value must be reduced to meet the requirement of the resonance condition. Figure 13 illustrates the decrease in the inductance L_1 when the ratio of the primary inductance C/C_c to the coupling capacitance increases gradually.

In summary, the value of the primary inductor, L_1 , can be calculated based on the resonance condition and relies on the value of the coupling plate, shield coupling plate, and load resistance. In addition, resonance can be achieved without the secondary inductor, L_2 , and becomes an advantage of the S-CPT system in terms of the weight. However, other conditions, such as a matching condition, voltage stress between the plates, and loss, need to be analyzed, and the results are presented in the next section.

4.2. Matching Condition of the Asymmetric S-CPT System

In a matching condition, the load R_L must be obtained by using the current magnitude $|I_1/V_i|$, as in Equation (9). As mentioned, the peak of the response must reach 0.01 at a 13.56 MHz operating frequency. Various loads R_L are presented in Figure 14.

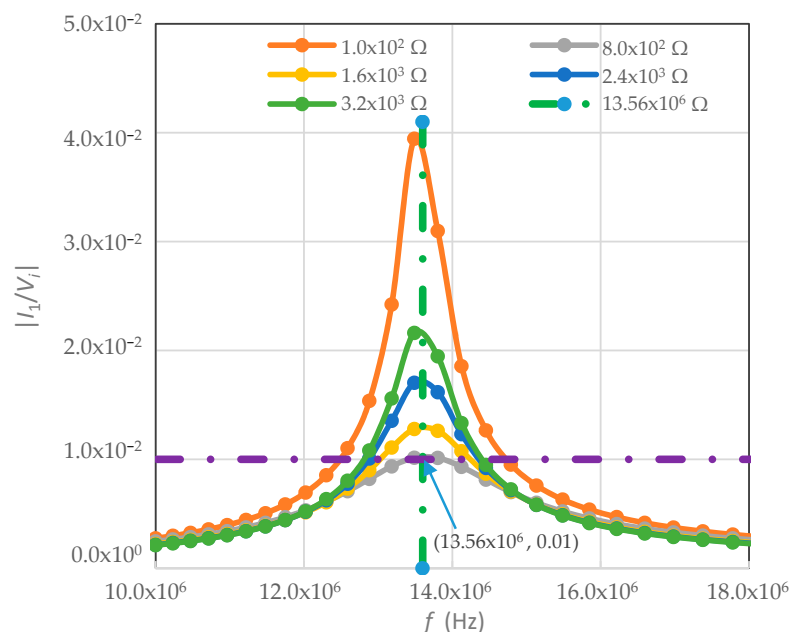


Figure 14. Response of $|I_1/V_i|$ at various loads.

Figure 14 shows the current response when the load $|I_1/V_i|$ changes. When the load is 800Ω , the circuit meets the matching condition with a peak of 0.01. The calculated inductance value for a load of 800Ω is $8.0 \mu\text{H}$. Thus, based on the calculation and analysis, S-CPT is under a matching condition with $L_2 = 0$ and a load of 800Ω for a 13.56 MHz operating frequency.

4.3. Voltage Stress Condition of the Asymmetric S-CPT System

The voltage stress between the coupling plate (V_B, V_A) and shield coupler at the primary V_A and secondary V_B of the asymmetric S-CPT was investigated by supplying a 1 V voltage with an operating frequency of 13.56 MHz . The voltage stress result is presented in Figure 15, which shows that a higher voltage stress occurred at the shield coupler plate at V_B . Thus, the breakdown voltage in this configuration occurs at the shield coupler plate, and the voltage stress is limited to 30 kV/cm .

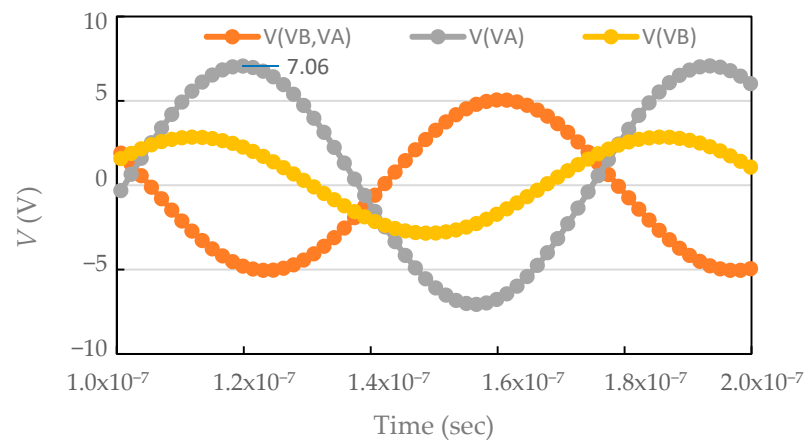


Figure 15. Voltage at the plates.

4.4. Efficiency of the Asymmetric S-CPT System

Considering the internal resistance in inductance, an approximation of the internal resistance of inductance, R_s , is included to find the loss in the asymmetric S-CPT system. The approximate results are presented in Figure 16.

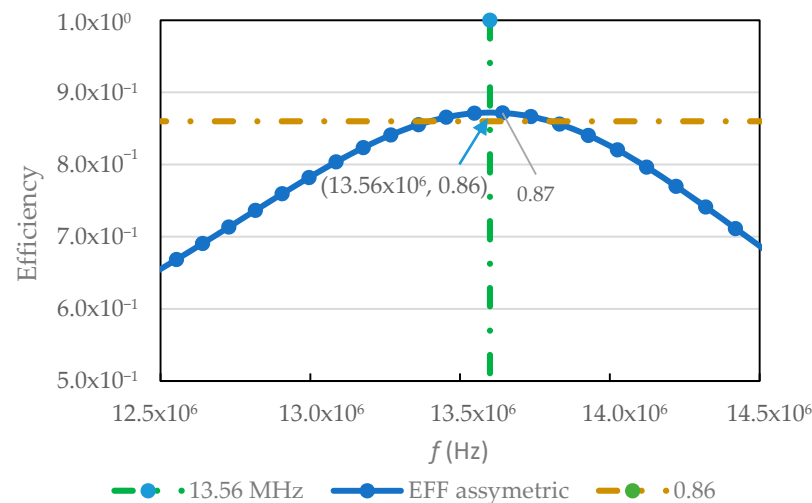


Figure 16. Efficiency in asymmetric S-CPT system with internal resistance.

Figure 16 shows the efficiency of asymmetric S-CPT with the primary inductor L_1 set to $8 \mu\text{H}$ and a load of 800Ω . The vertical graph is plotted with a value of 0.86 as

the maximum efficiency in the case of the symmetric S-CPT. The graph shows that the asymmetric S-CPT has better efficiency than the symmetric S-CPT.

In summary, all the analyses for primary inductance L_1 with secondary inductance $L_2 = 0$ were performed, and the results were obtained. The asymmetric S-CPT can be designed under resonance conditions and matching conditions with better efficiency. The ratio between the shield coupler capacitance C and the coupling capacitance C_C can be increased to minimize the value of the inductor L_1 .

5. Hardware Design of an Asymmetric S-CPT

Based on the findings of the analysis, which covered the resonance condition, matching circuit condition, electric field limitation, and power loss, an asymmetric S-CPT system was designed. The parameters of the asymmetric components were chosen, as shown in Table 3, and the value of the primary inductor L_1 was calculated using Equation (7). Table 3 shows the design value is obtained using the analysis result. The measurement value was acquired from the measurement of the hardware in which the hardware was fabricated to the closest value of the calculated design. By using $|I_1/V_i|$ curved as in Equation (8), the impedance match was approximated at a load of 400Ω at an operating frequency of 13.56 MHz.

Table 3. Parameters of S-CPT based on the design value and measurement value.

| Parameter | Symbol | Design Value | Measurement Value |
|-----------------------------------|--------|--------------------------|---------------------------|
| Operating frequency | f | 13.56×10^6 Hz | 13.56×10^6 Hz |
| Primary inductor | L_1 | 5.53×10^{-6} H | 5.60×10^{-6} H |
| Coupling capacitance | C_c | 12.0×10^{-12} F | 12.50×10^{-12} F |
| Primary shield coupling primary | C_1 | 15.0×10^{-12} F | 15.10×10^{-12} F |
| Secondary shield coupling primary | C_2 | 15.0×10^{-12} F | 15.23×10^{-12} F |
| Load | R_L | 400Ω | 400Ω |

The coupler plate was designed using an area of 60×100 mm with an FR4 printed circuit board, and the gap between the couplers was adjusted until the measurement value provided the closest value of the design capacitance. Inductance was created using an air-core-type inductor, and the setup is shown in Figure 17.

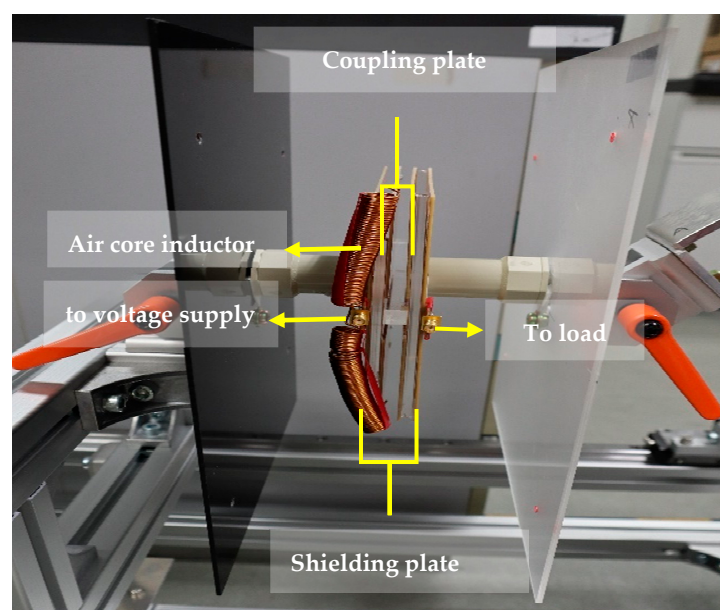


Figure 17. Experimental setup for S-CPT system.

The hardware values of both the capacitance and the inductor are listed in Table 1 as the measurement values. The measurement data for the inductor, coupling plate capacitance, and shield coupler plate were obtained using an Agilent 4294A impedance analyzer at 13.56 MHz. The experimental setup of the asymmetric test hardware is depicted in Figure 17, which shows the two air-core inductors used, and six plates were used to form the capacitive coupler and capacitive shield coupler.

6. Results and Discussion

The S-CPT system was analyzed based on efficiency and impedance matching, and the results from the analyzed design and fabricated hardware are presented in Figure 18.

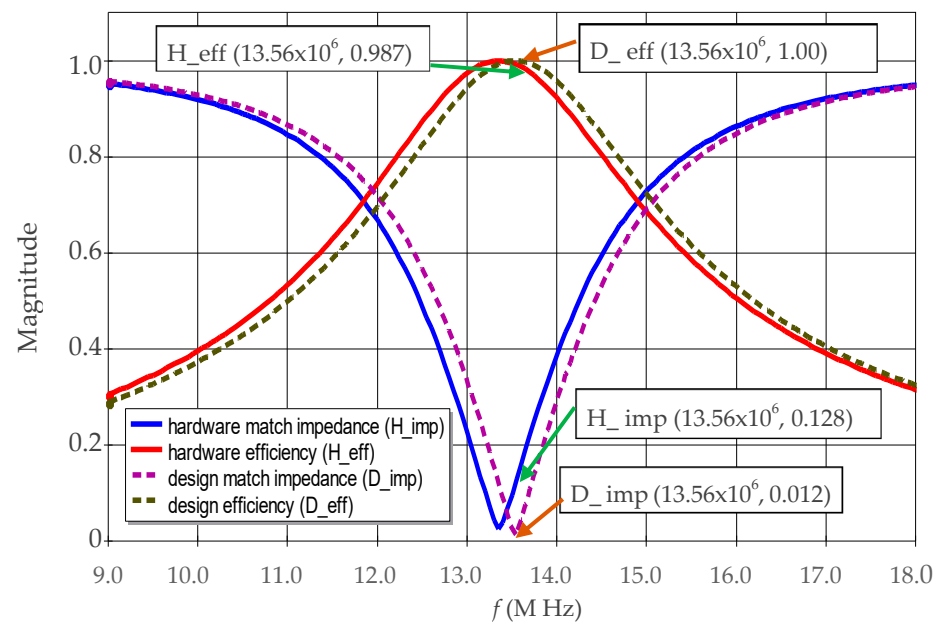


Figure 18. Efficiency and matching impedance for design and hardware.

In an ideal S-CPT case, the efficiency and matching impedance are 1 and 0, respectively. Figure 18 shows the result of the hardware S-CPT at 13.56 MHz, which gives an efficiency of 0.987 or 98.7% and impedance match of 0.128. Considering the ideal matching impedance condition as in the analysis section, current $|I_1/V_i|$ of the hardware S-CPT is 0.01 when the obtained impedance match in the measurement is 0. Therefore, the response $|I_1/V_i|$ of the hardware S-CPT is not exactly 0.01, as indicated by the impedance match value of 0.128. The hardware S-CPT has the reflected voltage though the transmitter, which leads to an imperfect matching impedance condition. This may be due to the slight imprecision of the hardware fabrication process.

The difference in the value of the hardware compared with the design value is caused by the imprecision of fabricating the actual capacitance coupler and inductor. Moreover, misalignment tolerance during installation of the hardware S-CPT was also affected by the result. Based on the results presented in Figure 18, the measurement was reconfirmed by the test equipment, and the results are presented in Figures 19–21.

Figure 19 shows the efficiency when a voltage with an operating frequency of 13.56 MHz is supplied to the S-CPT. The resulting graph shows that the efficiency obtained is 0.98 or 98%. The result confirms that the hardware S-CPT based on the analysis was designed successfully.

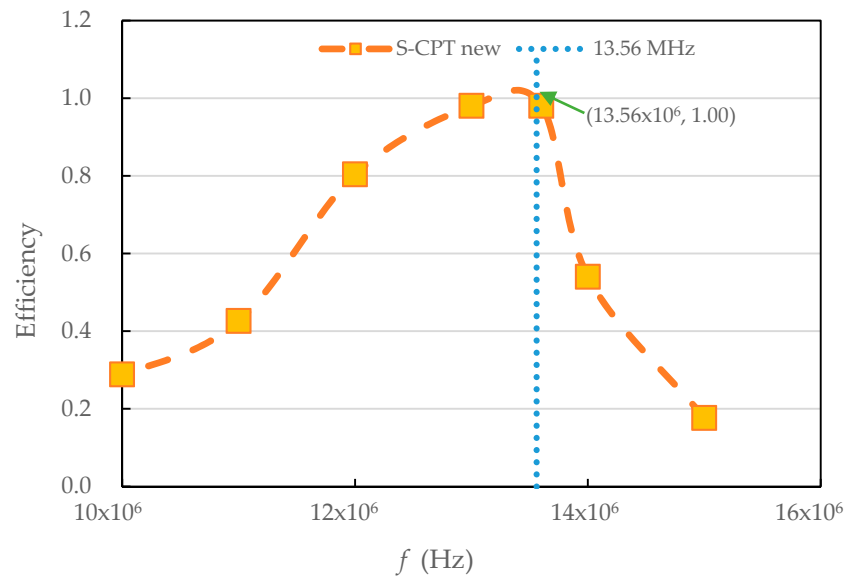


Figure 19. Efficiency of S-CPT system at various frequencies.

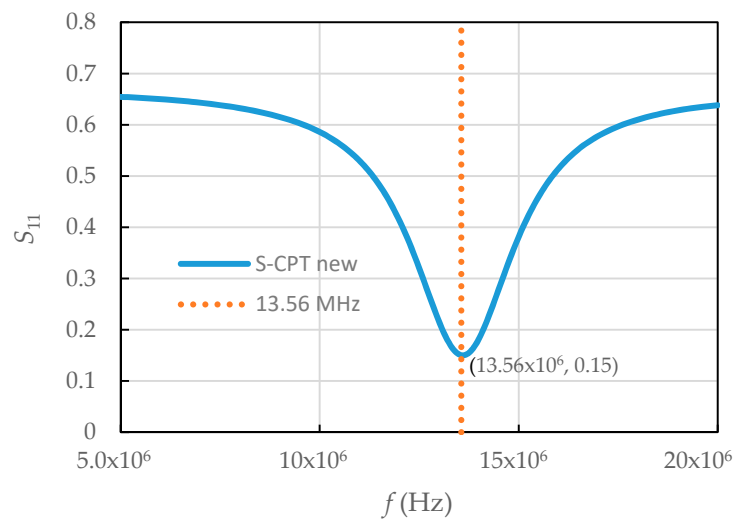


Figure 20. Impedance matching of S-CPT system at various frequencies.

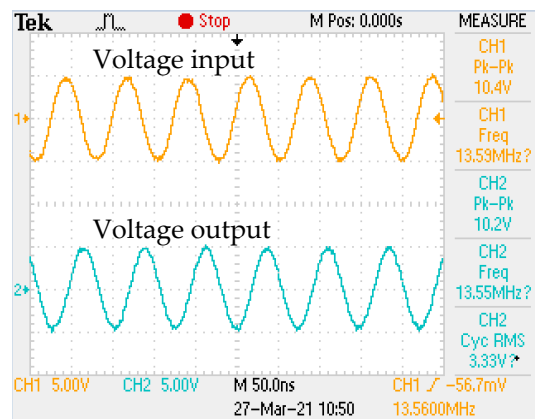


Figure 21. Voltage at the load of the S-CPT system.

Figure 20 shows the impedance matching of the asymmetric S-CPT system at various frequencies. It shows that the impedance match magnitude value approaches 0.15 at a 13.56 MHz operating frequency. Considering Figure 18, the obtained impedance match value is almost same for both measurements with a difference of 0.022. The measurement of transferring voltage is done for both the input and output of the S-CPT system, as shown in Figure 21. AC voltage with a frequency of 13.56 MHz is supplied to obtain the output voltage of S-CPT. Figure 21 shows the obtained input voltage and output voltage are 10.4 V and 10.2, respectively. The result shows that the asymmetric S-CPT system can transfer the voltage from the input to the load with a voltage peak reduction of almost 2%.

7. Conclusions

A generalized model of S-CPT was successfully developed by using an algebraic method. Symmetric and asymmetric S-CPT configurations with an operating frequency of 13.56 MHz were analyzed with respect to the resonance condition, matching conditions, electric field, and efficiency.

In a symmetric S-CPT system, the generalized model can be used as a comprehensive method to determine the parameters for achieving the minimum value of the inductor, good design stability, and high efficiency. A recommended symmetric S-CPT configuration was also provided. The two values of the primary inductor L_1 and secondary inductor L_2 were based on the desired specification. In terms of low cost and weight, $L_1 = L_2 = 4.74 \mu\text{H}$ is recommended. However, in terms of stability in the resonance condition and the power loss, $L_1 = L_2 = 9.19 \mu\text{H}$ is an option.

In the asymmetric S-CPT system, there is no secondary inductor L_2 . The resultant weight, loss, and cost can be reduced. The analysis results show that a good asymmetric S-CPT design can be achieved with better efficiency. An experimental hardware setup was used to investigate the validity of the generalized model based on the analysis method for designing the S-CPT system. The experimental results show that the proposed method is effective for designing an S-CPT system. Thus, the proposed generalized model is recommended for the design of an S-CPT system.

Author Contributions: Conceptualization and methodology, S.A., R.H., and A.M.; validation, S.A. and R.H.; hardware experiments, S.A.; writing—original draft preparation, S.A.; writing—review and editing, S.A., R.H., and A.M.; supervision, R.H. and A.M. All authors have read and agreed to the published version of the manuscript.

Funding: This research received no external funding.

Institutional Review Board Statement: Not applicable.

Informed Consent Statement: Not applicable.

Data Availability Statement: Not applicable.

Acknowledgments: The authors would like to thank members of Automotive System and Device Laboratories, Furukawa Electric Co., Ltd. for their technical support and the Ministry of Higher Education (MOHE) Malaysia and Universiti Teknikal Malaysia Melaka for the SLAB scholarship support to S.A.

Conflicts of Interest: The authors declare no conflict of interest.

References

1. Ahmad, A.; Alam, M.S.; Chabaan, R. A Comprehensive review of wireless charging technologies for electric vehicles. *IEEE Trans. Transp. Electrification*. **2017**, *4*, 38–63. [[CrossRef](#)]
2. Muharam, A.; Ahmad, S.; Hattori, R.; Hapid, A. 13.56 MHz scalable shielded-capacitive power transfer for electric vehicle wireless charging. In Proceedings of the 2020 IEEE PELS Workshop on Emerging Technologies: Wireless Power Transfer (WoW), Seoul, Korea, 15–19 November 2020; pp. 298–303. [[CrossRef](#)]
3. Dai, J.; Ludois, D.C. Capacitive power transfer through a conformal bumper for electric vehicle charging. *IEEE J. Emerg. Sel. Top. Power Electron.* **2016**, *4*, 1015–1025. [[CrossRef](#)]

4. Regensburger, B.; Sinha, S.; Kumar, A.; Vance, J.; Popovic, Z.; Afridi, K.K. Kilowatt-scale large air-gap multi-modular capacitive wireless power transfer system for electric vehicle charging. In Proceedings of the 2018 IEEE Applied Power Electronics Conference and Exposition (APEC), San Antonio, TX, USA, 4–8 March 2018; pp. 666–671. [[CrossRef](#)]
5. Narayanamoorthi, R. Modeling of capacitive resonant wireless power and data transfer to deep biomedical implants. *IEEE Trans. Compon. Packag. Manuf. Technol.* **2019**, *9*, 1253–1263. [[CrossRef](#)]
6. Park, C.; Park, J.; Shin, Y.; Kim, J.; Huh, S.; Kim, D.; Ahn, S.; Park, S. Separated circular capacitive coupler for reducing cross-coupling capacitance in drone wireless power transfer system. *IEEE Trans. Microw. Theory Tech.* **2020**, *68*, 3978–3985. [[CrossRef](#)]
7. Mostafa, T.M.; Muharam, A.; Hattori, R. Wireless battery charging system for drones via capacitive power transfer. In Proceedings of the 2017 IEEE PELS Workshop on Emerging Technologies: Wireless Power Transfer (WoW), Chongqing, China, 20–22 May 2017. [[CrossRef](#)]
8. Yusop, Y.; Saat, S.; Ghani, Z.; Husin, H.; Adie, M.K.; Nguang, S.K. Cascaded boost-class-e for rotary capacitive power transfer system. *J. Eng.* **2019**, *2019*, 3742–3748. [[CrossRef](#)]
9. Ahmad, S.; Muharam, A.; Hattori, R. Rotary capacitive power transfer with class-E inverter and balun circuit. In Proceedings of the 2020 IEEE PELS Workshop on Emerging Technologies: Wireless Power Transfer (WoW), Seoul, Korea, 15–19 November 2020; pp. 330–333. [[CrossRef](#)]
10. Dai, J.; Hagen, S.; Ludois, D.C.; Brown, I.P. Synchronous generator brushless field excitation and voltage regulation via capacitive coupling through journal bearings. *IEEE Trans. Ind. Appl.* **2017**, *53*, 3317–3326. [[CrossRef](#)]
11. Di Gioia, A.; Brown, I.; Nie, Y.; Knippel, R.; Ludois, D.; Dai, J.; Hagen, S.; Altheld, C. Design of a wound field synchronous machine for electric vehicle traction with brushless capacitive field excitation. In Proceedings of the IEEE Energy Conversion Congress and Exposition 2016 IEEE, Milwaukee, WI, USA, 18–22 September 2016; Volume 54, pp. 1–8.
12. Lu, F.; Zhang, H.; Mi, C. A review on the recent development of capacitive wireless power transfer technology. *Energies* **2017**, *10*, 1752. [[CrossRef](#)]
13. Liu, C.; Hu, A.P.; Budhia, M. A generalized coupling model for capacitive power transfer systems. In Proceedings of the IECON 2010 36th Annual Conference on IEEE Industrial Electronics Society, Glendale, AZ, USA, 7–10 November 2010; pp. 274–279. [[CrossRef](#)]
14. Minnaert, B.; Costanzo, A.; Monti, G.; Mongiardo, M. Capacitive wireless power transfer with multiple transmitters: Efficiency optimization. *Energies* **2020**, *13*, 3482. [[CrossRef](#)]
15. Wang, S.; Liang, J.; Fu, M. Analysis and design of capacitive power transfer systems based on induced voltage source model. *IEEE Trans. Power Electron.* **2020**, *35*, 10532–10541. [[CrossRef](#)]
16. Corti, F.; Reatti, A.; Wu, Y.-H.; Czarkowski, D.; Musumeci, S. Zero voltage switching condition in class-e inverter for capacitive wireless power transfer applications. *Energies* **2021**, *14*, 911. [[CrossRef](#)]
17. Lu, F.; Member, S.; Zhang, H.; Member, S.; Hofmann, H.; Member, S. A Double-Sided LC compensation circuit for loosely-coupled capacitive power transfer. *IEEE Trans. Power Electron.* **2017**, *33*, 1–10. [[CrossRef](#)]
18. Lu, F.; Zhang, H.; Hofmann, H.; Mi, C. A Double-sided LCLC-compensated capacitive power transfer system for electric vehicle charging. *IEEE Trans. Power Electron.* **2015**, *30*, 6011–6014. [[CrossRef](#)]
19. Zhang, H.; Lu, F.; Hofmann, H.; Liu, W.; Mi, C.C. A four-plate compact capacitive coupler design and LCL-compensated topology for capacitive power transfer in electric vehicle charging application. *IEEE Trans. Power Electron.* **2016**, *31*, 8541–8551. [[CrossRef](#)]
20. Zhu, Q.; Zou, L.J.; Su, M.; Hu, A.P. Four-plate capacitive power transfer system with different grounding connections. *Int. J. Electr. Power Energy Syst.* **2020**, *115*, 105494. [[CrossRef](#)]
21. Zhang, H.; Lu, F.; Hofmann, H.; Liu, W.; Mi, C.C. An LC-compensated electric field repeater for long-distance capacitive power transfer. *IEEE Trans. Ind. Appl.* **2017**, *53*, 4914–4922. [[CrossRef](#)]
22. Li, S.; Liu, Z.; Zhao, H.; Zhu, L.; Shuai, C.; Chen, Z. Wireless power transfer by electric field resonance and its application in dynamic charging. *IEEE Trans. Ind. Electron.* **2016**, *63*, 6602–6612. [[CrossRef](#)]
23. Zhang, H.; Lu, F.; Hofmann, H.; Liu, W.; Mi, C.C. Six-plate capacitive coupler to reduce electric field emission in large air-gap capacitive power transfer. *IEEE Trans. Power Electron.* **2018**, *33*, 665–675. [[CrossRef](#)]
24. Muharam, A.; Ahmad, S.; Hattori, R. Scaling-factor and design guidelines for shielded-capacitive power transfer. *Energies* **2020**, *13*, 4240. [[CrossRef](#)]
25. Muharam, A.; Ahmad, S.; Hattori, R.; Obara, D.; Masuda, M.; Ismail, K.; Hapid, A. An improved ground stability in shielded capacitive wireless power transfer. In Proceedings of the 2019 International Conference on Sustainable Energy Engineering and Application (ICSEEA), Tangerang, Indonesia, 23–24 October 2019; pp. 16–20. [[CrossRef](#)]
26. Regensburger, B.; Kumar, A.; Sinha, S.; Doubleday, K.; Pervaiz, S.; Popovic, Z.; Afridi, K. High-performance large air-gap capacitive wireless power transfer system for electric vehicle charging. In Proceedings of the 2017 IEEE Transportation Electrification Conference and Expo (ITEC), Chicago, IL, USA, 22–24 June 2017; pp. 638–643. [[CrossRef](#)]
27. Lu, F.; Zhang, H.; Hofmann, H.; Mi, C.C. An inductive and capacitive integrated coupler and its LCL compensation circuit design for wireless power transfer. *IEEE Trans. Ind. Appl.* **2017**, *53*, 4903–4913. [[CrossRef](#)]
28. Mostafa, T.M.; Bui, D.; Muharam, A.; Hu, A.P.; Hattori, R. Load effect analysis and maximum power transfer tracking of CPT system. *IEEE Trans. Circuits Syst. I Regul. Pap.* **2020**, *67*, 2836–2848. [[CrossRef](#)]

-
29. Zhou, Q.; Wen, M.; Xiong, T.; Jiang, T.; Zhou, M.; Ouyang, X.; Xing, L. Study on insulation breakdown characteristics of printed circuit board under continuous square impulse voltage. *Energies* **2018**, *11*, 2908. [[CrossRef](#)]
 30. Tang, L.; Ruan, J.; Qiu, Z.; Huang, D.; Wei, M.; Huang, C. Breakdown voltage calculation of sphere-planesphere air gap in slightly uneven electric field. In Proceedings of the 2016 IEEE International Conference on High Voltage Engineering and Application (ICHVE), Chengdu, China, 19–22 September 2016; p. 3.